Polymer 51 (2010) 1516–1523

Contents lists available at ScienceDirect

Polymer

journal homepage: www.elsevier.com/locate/polymer

Crystallization, and morphology of poly(trimethylene terephthalate)/poly(ethylene oxide terephthalate) segmented block copolymers

Chenguang Yao [a,b], Guisheng Yang [a,c,*]

[a] CAS Key Laboratory of Engineering Plastics, Joint Laboratory of Polymer Science and Technology, Institute of Chemistry, the Chinese Academy of Sciences, Beijing 100080, PR China
[b] Graduate University of the Chinese Academy of Sciences, Beijing 100039, PR China
[c] Shanghai Genius Advanced Material Co., Ltd., Shanghai 201109, PR China

ARTICLE INFO

Article history:
Received 9 August 2009
Received in revised form
9 December 2009
Accepted 20 January 2010
Available online 28 January 2010

Keywords:
Poly(trimethylene terephthalate)
Poly(ether–ester)
Dendritic crystals

ABSTRACT

A new type of poly(ether–ester) based on poly(trimethylene terephthalate) as rigid segments and poly(ethylene oxide terephthalate) as soft segments was synthesized and its crystallization behavior and morphology were investigated. Differential Scanning Calorimetry revealed that the copolymer containing 57 wt% soft segments presented a low glass transition temperature (−46.4 °C) and a high melting temperature (201.8 °C), suggesting that it had the typical characteristic of thermoplastic elastomer. With increasing soft segment content from 35 to 57 wt%, the crystallization morphology transformed from banded spherulites to compact seaweed morphology at a certain film thickness, which was due to the change of surface tension and diffusivity caused by increasing the soft segment content. Moreover, with the decrease of film thickness from 15 to 2 μm, the crystallization morphology of the copolymer (57 wt% soft segment) changed from wheatear-like, compact seaweed to dendritic. Scanning Electron Microscopy revealed that some flower-like crystals presenting in the bulk, which had been surprisingly found in the poly(ether–ester) segmented block copolymers for the first time. Possible mechanism was discussed in the text.

1. Introduction

Segmented block copolymers are often composed of flexible and rigid segments. Due to structural differences, the flexible and rigid segments usually separate into two phases or domains. At room temperature, the segmented block copolymers have multi-phase structures consisting of a continuous phase of the flexible segments with a low glass transition temperature and a dispersed phase with a high melting temperature [1]. Soft phase provides extensibility, whereas hard domains play the role of physical cross-links and act as high modulus filler. Segmented block copolymer is a subcategory of thermoplastic elastomers (TPEs) with multi-alternating blocks, which can be expressed by a general formula $(—A—B—)_n$ [2]. Polyurethane, poly(ether–ester), and poly(ether–amide) belong to this category.

Crystallization of the rigid segments is possible if their structure is regular, as for certain polyurethane, polyester and polyamide segments block copolymers [1]. Two crystallization morphologies, spherulites [3–5] and ribbon-like crystallites [6–10] of segmented copolymers have been reported. The spherulites in segmented polyurethanes are formed by fibrils that are more densely packed in the center. Ribbon-like crystallites are usually observed for the copolymers with monodispersed hard segments. A series of diblock and triblock copolymers with monodispersed hard segments have been prepared by Gaymans et al. [6–10]. The morphology of these copolymers consists of uniform thin crystalline ribbons with high aspect ratios. These nano-ribbon crystallites serve as the physical cross-links for the soft phase and also reinforce the soft phase. Different from diblock copolymers [11–17] and triblock copolymer [18–20], multiblock block copolymers are complicated systems due to structural heterogeneity arising from the distribution of the hard segment lengths and even the possible existence of hard segment homopolymers [3].

Multiblock poly(ether–ester) (PEE) based on poly(butylene terephthalate) (PBT) as rigid segments and poly(tetramethylene oxide) (PTMO) as soft segments have been intensively studied [21–24], being available as commercial products (Elitel™, Elana; Arnitel, Hytrel®, Du Pont; DSM, etc.). Poly(trimethylene terephthalate) (PTT) is a newly commercialized aromatic polyester, which possesses an unusual combination of the topping properties of PET and the

* Corresponding author at: CAS Key Laboratory of Engineering Plastics, Joint Laboratory of Polymer Science and Technology, Institute of Chemistry, the Chinese Academy of Sciences, Beijing 100080, PR China. Tel.: +86 21 64881869.
E-mail address: ygs@geniuscn.com (G. Yang).

0032-3861/$ – see front matter © 2010 Elsevier Ltd. All rights reserved.
doi:10.1016/j.polymer.2010.01.045

processing characteristics of PBT. Therefore, it has become one of the most important polymer materials recently. Moreover, PTT shows various crystallization morphologies, such as regular spherulites, weakly banded spherulites, banded spherulites [25–27], even alternating-layered spherulites [28]. However, little work has focused on the crystallization morphology of PTT copolymer while copolymers possess rich morphological textures [29].

Crystallization of block copolymer micro-domains exerts tremendous influence on the morphology, properties and applications of these materials. Actually, in polyester-segmented block copolymers, the phase separation occurs mainly by crystallization [1]. In this study, poly(trimethylene terephthalate-block-ethylene oxide terephthalate) (PTT/PEOT) copolymers were synthesized. The influence of soft segment content on crystallization and morphology, as well as the effect of film thickness on morphology of copolymers were investigated. Different from multiblock block copolymers with PBT or PET as rigid segments, the poly(ether–ester) with PTT as rigid segments exhibits different crystallization morphologies. Possible mechanism was discussed based on the previous theory and experimental results. To the best of our knowledge, this is the first time that the crystallization morphology of PEE with PTT as rigid segments and PEOT as soft segments was investigated.

2. Experimental

2.1. Materials

Dimethyl terephthalate (DMT, Shanghai Chemical Reagent Co., China, 99%), 1,3-propanediol (PDO, Heilongjiang Chenneng Bioengineering Co. LTD, China, 99.9%) and poly(ethylene glycol) (PEG, Fluka, USA, 99.9%) with molecular weight 2000 g/mol were used to synthesize PTT/PEOT copolymer. Zinc acetate and tetrabutyl titanate (Aldrich) were used as catalysts in transesterification and polycondensation. Irganox 1330 (Aldrich) was used as antioxidant. All materials were used without further purification.

2.2. Polymerization

PTT/PEOT multiblock copolymers were synthesized by traditional melt transesterification and subsequently polycondensation as follows. Transesterification was performed in two stages. In the first stage, a mixture of DMT, PDO, with a small amount of catalyst (0.20 wt% in relation to DMT) was charged into well dried 250 ml three-necked round-bottom flask under nitrogen atmosphere. The flask equipped with a mechanical stirrer, a nitrogen inlet and a distillation column. The mixture was stirred continuously throughout the reaction for about 2 h at 190 °C. In the next stage, PEG is introduced to the flask, together with second portion catalyst (0.10 wt% in relation to DMT) and an antioxidant (0.5% of total comonomers mass), and the reaction mixture was heated slowly to 225 °C and stayed for about 1.5 h to reach the endpoint of transesterification. Finally, the mixture was heated to 255 °C for 3 h under the pressure of about 20 Pa. The product was cooled to room temperature, repeatedly washed by water, and dried under a vacuum at 70 °C for 1 day to obtain the PTT/PEOT copolymers. Pristine PTT was synthesized under the same reaction conditions as the above procedure without loading PEG. Corresponding to theoretical hard segment content (HSC), the copolymers were designated as A0 (100% HSC), A1 (60% HSC), A2 (40% HSC).

2.3. Characterization

All the copolymers investigated were purified by dissolution in the mixed solvent of chloroform and 1,1,1,3,3,3-hexafluoro-2-propanol (95:5 w/w) and precipitation into excess of ethanol.

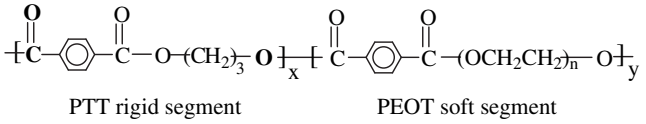

Fig. 1. Chemical structure of PTT/PEOT segmented copolymers.

The intrinsic viscosities [η] of these samples in mixed solvent of phenol and 1,1,2,2-tetrachloroethane (60:40 w/w) were determined at 30 °C using an Ubbelohde viscometer.

^{1}H NMR spectra of the copolymer were recorded on a Bruker ASPECT 300 Hz spectrometer at room temperature. Each of the copolymer was dissolved in CF_3COOD. Tetramethylsilane was used as the standard reference material for ^{1}H NMR spectra. The resultant HSC of the copolymer was calculated from the data obtained from these spectra.

The melting and crystallization behaviors of all the samples were investigated with the following program: the dried samples were first heated at a heating rate of 50 °C/min from room temperature to 250 °C under a nitrogen atmosphere, held for 3 min and cooled to −100 °C at a cooling rate of 200 °C/min, then heated again at a rate of 20 °C/min to 260 °C, held for 3 min, and cooled back to 30 °C at a rate of 20 °C/min. The second heating and cooling processes were recorded with a PerkinElmer Diamond DSC instrument (Shelton, CT).

The crystallization morphology of PTT was observed by using Polarized Optical Microscopy (POM) (Olympus BX51-P.) coupled with a computer-controlled CCD camera (Tota, Japan). A dual hot stage (KH-08, kangsente Co., China) was employed for controlling the temperature. The hot stage contains two stages, whose temperature can be controlled separately, i.e., one is for polymer melting and the other for crystallization. The specimens, sandwiched between two clean glass slides, were first melted at 250 °C for 5 min, spread by sliding the substrates into opposite directions, and then quickly transferred to the second stage for crystallization, held for a certain time. The second stage has been pre-heated to the desired crystallization temperature (T_c). The hot stage was charged with nitrogen. The POM micrographs were captured either during crystallization process or at room temperature. The film thickness was controlled by a previous reported method [30] and measured either by optical microscopy or atomic force microscopy.

The morphology of copolymers either crystallized or stretched was characterized by a JSM-6700F field emission scanning electron microscope (FE-SEM) (Japan).

Wide-Angle X-ray Diffraction (WAXD) was carried out by a Rigaku X-ray diffractometer with a Nifiltered Cu Kα radiation ($\lambda = 0.1546$ nm) at room temperature. The scan rate was 4° 2 θ/min. The selected voltage and current were 40 kV and 200 mA, respectively.

3. Results and discussion

3.1. Preparation and characterization of PTT/PEOT copolymers

The thermoplastic poly(ether–ester) copolymers based on poly(trimethylene terephthalate) PTT as rigid segment, and poly(ethylene oxide terephthalate) (PEOT) as soft segment were synthesized by a traditional two-stage melt transesterification and polycondensation. The final products are linear multiblock copolymers with random distribution of the rigid and soft segments. The chemical structure of the segmented PTT/PEOT is shown in Fig. 1. Two copolymers with theoretical HSC 40 and 60 wt% were fabricated. However, the experimental HSC is not always consistent with

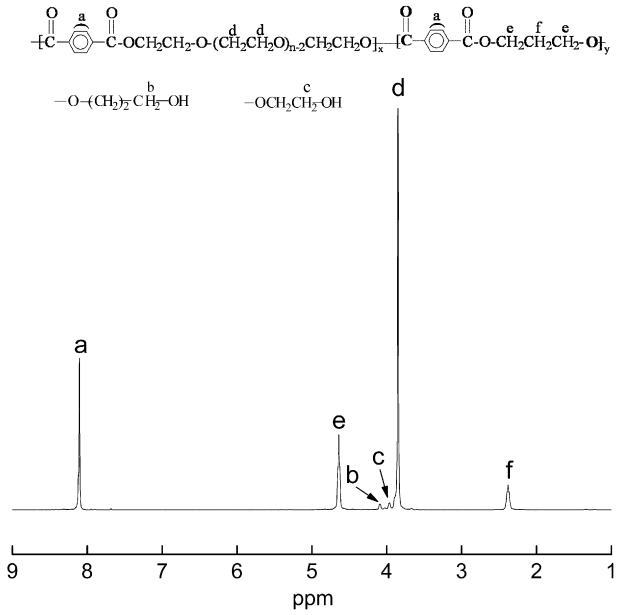

Fig. 2. ^{1}H NMR spectra of the segmented copolymer (A2).

the theoretical value, so ^{1}H NMR spectra was employed to determine the resultant HSC in the copolymer.

Fig. 2 presents the ^{1}H NMR spectra of the segmented copolymer (A2) along with peak assignments. The strong peak at 3.85 ppm (peak d) corresponds to the signals of the proton on the carbon atoms connected with oxygen CH_2–O–CH_2 of the PEO repeating blocks. The signal at 8.11 ppm (peak a) corresponds to the aromatic proton of the terephthalate units. The chemical shifts at 4.64 (peak e) and 2.38 ppm (peak f) are for the methylene protons of the short chain diol. Small signal at 4.09 (peak b) and at 3.96 ppm (peak c) are due to the protons of methylene in CH_2–OH end groups of polyester and polyether, respectively. The bands at 3.85, 4.64 and 8.11 ppm were used for the compositional calculation. The weight ratio of hard and soft segments (w_h/w_s) can be obtained by solving Eq. (1). The hard segment content can be calculated according to Eq. (2).

$$\frac{(w_h \times 4)/206}{(w_s/2130) \times (2000/44) \times 4} = \frac{I_e}{I_d} \quad (1)$$

$$W_h = \frac{w_h}{w_h + w_s} \times 100\% \quad (2)$$

where 2130 and 206 are the molecular weight of the soft polyether and rigid polyester chain repeat unites, respectively. 2000 and 44 are the molecular weight of PEG and –CH_2–CH_2–OH segment, respectively. I_d and I_e are the integral intensities of d and e peaks, respectively. The average length of the hard segments were calculated from the ratio (d:a) of the peak intensities, based on the assumption that the soft segment length is equal to the length of the staring PEO. Detailed calculation method can be found in the literature [31,32]. The number average molecular weights (M_n), hard segment content and length are listed in Table 1. It is obvious that the resultant hard segment content in the copolymer is a little higher than the theoretical one. The intrinsic viscosities of the two segmented copolymers and PTT are also listed in Table 1.

Table 1
Characteristic data for neat PTT and the segmented copolymers.

Samples	W_h (%)		$L_{n,h}$		$[\eta]$	M_n
	Theory	By NMR	Theory	By NMR	dl/g	g/mol
A0	–	–	–	–	0.81	20,262[a]
A1	60	65.0	7.6	7.4	1.19	14,523[b]
A2	40	42.7	3.7	3.6	1.53	12,785[b]

W_h (%)-hard content by weight; $L_{n,h}$-average length of hard segment.
[a] determined from $[\eta]$.
[b] determined from ^{1}H NMR spectra.

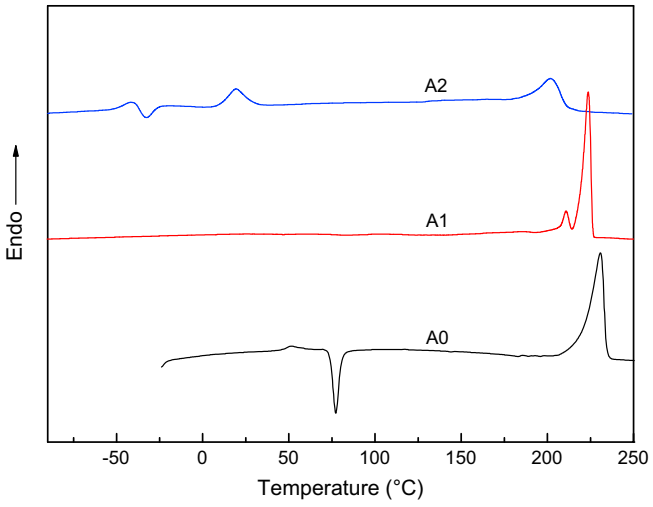

Fig. 3. Second heating DSC curves of pure PTT and the segmented copolymers.

3.2. DSC analysis

Typical melting DSC curves of the three samples are shown in Fig. 3. The DSC parameters of the melting process are summarized in Table 2. Pure PTT exhibits an apparent glass transition temperature (T_g) at about 48.3 °C, a cold-crystallization peak ($T_{c,c}$) at about 77.1 °C, and a melting peak (T_m) at about 230.7 °C. The segmented copolymer which contains 65 wt% hard segment (A1) only exhibits a double melting peak. With decreasing hard segment content, the segmented copolymer reveals a complex endotherm. That is, A2 exhibits four transitions: T_m of hard segment at 201.8 °C, as well as T_g, $T_{c,c}$, T_m of soft segment at −46.4, −32.8 and 19.3 °C, respectively. The melting temperature of the hard segments depends strongly on the average sequence length of hard segment. An increase in PTT weight fraction results in

Table 2
DSC parameters of melting and crystallization for neat PTT and segmented copolymers.

Sample	Heating scan							Cooling scan	
	$T_{g,s}$ (°C)[a]	$T_{c,c,s}$ (°C)[b]	$T_{m,s}$ (°C)[c]	$T_{g,h}$ (°C)[d]	$T_{c,c,h}$ (°C)[e]	$T_{m,h}$ (°C)[f]	$\Delta H_{m,h}$ (J/g)[g]	$T_{m,c}$ (°C)[h]	ΔH_c (J/g)[i]
A0	–	–	–	48.3	77.1	230.7	43.2	177.7	−48.0
A1	–	–	–	–	–	223.9	30.9	173.2	−37.8
A2	−46.4	−32.8	19.3	–	–	201.8	19.3	158.5	−17.8

The subscript letters 's' and 'h' indicate 'soft segment' and 'hard segment', respectively.
[a] Glass-transition temperature of soft segment.
[b] Cold-crystallization temperature of soft segment.
[c] Melting temperature of soft segment.
[d] Glass-transition temperature of hard segment.
[e] Cold-crystallization temperature of hard segment.
[f] Melting temperature of hard segment.
[g] Melting enthalpy of hard segment.
[h] Crystallization temperature of copolymers.
[i] Crystallization enthalpy of copolymers.

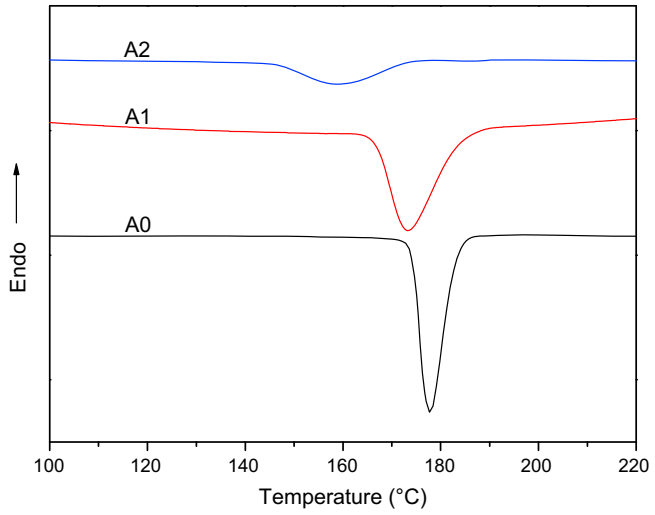

Fig. 4. Melt-crystallization DSC curves of pure PTT and the segmented copolymers.

higher melting temperature and an increase in the heat of fusion of the copolymer. In detail, the T_ms of the copolymers increase from 201.8 to 223.9 °C, and ΔH_m increase from 19.3 to 30.9 J/g, with increasing hard segment content from 42.7 wt% to 65.0 wt%. Moreover, T_m peak of A2 is relatively broad compared with A1 and the PTT homopolymer, due to the random condensation process during synthesis, which leads to the formation of chains with a distribution of PTT sequence lengths [31].

The thermoplastic and elastic behaviors of the polymer arise from their multi-phase structure due to the incompatibility of the two blocks (soft and hard) built into polymer chains. For PTT/PEOT copolymers containing 57.3 wt% soft segments, a low-T_g and a high-T_m can be observed, which suggests that it could be used as thermoplastic elastomers. In addition, recrystallization and melting peaks of PEOT fraction could be detected at −32.8 and 19.3 °C, respectively. So we can draw the conclusion that, at room temperature, A2 has two-phase construction: a PTT semi-crystalline phase and a polyether amorphous phase.

The melt–crystallization behaviors of three samples at the cooling rate of 20 °C/min are shown in Fig. 4, and the DSC parameters of the cooling process are also summarized in Table 2. As shown in Fig. 4, the crystallization temperature ($T_{m,c}$) of copolymers shift to lower temperature (173.2 °C for A1, 158.5 for A2) compared to PTT homopolymer (177.7 °C). Moreover, the crystallization exotherm of copolymers shows gradual widening in the range with increasing soft segment content, which suggests a gradual prolonged crystallization time. With increasing soft segment content, the chain motion of hard segment is considerably restricted compared to the corresponding homopolymer. Therefore, it will take more time for PTT chains move to the growing crystal front.

In fact, the hard segments of the PTT/PEOT segmented copolymers can not only crystallized but also grow into spherulites (or other morphology) superstructure as shown below.

3.3. Polarized optical microscopy (POM)

Fig. 5(a–c) shows three POM micrographs for A0, A1 and A2 isothermally crystallized at 150 °C for 30 min. It should be note that all the crystals studied in this paper grow with one free surface. The film thickness for A0–A2 was measured to be 15.6, 15.4 and 15.1 μm, respectively. Both Fig. 5(a) and (b) reveal the well-defined banded spherulites morphology. Spherulites impinge on one another and form particular polygonal spherulites with clear boundaries. The spherulites diameters in Fig. 5(a) and (b) are 80–200 and 60–90 μm, respectively. The band spacings in Fig. 5(a) and (b) are 2.1 and 2.3 μm, respectively. At the same time, the copolymer with 57.3 wt% soft segment (A2) also exhibits a spherulitic morphology. By careful

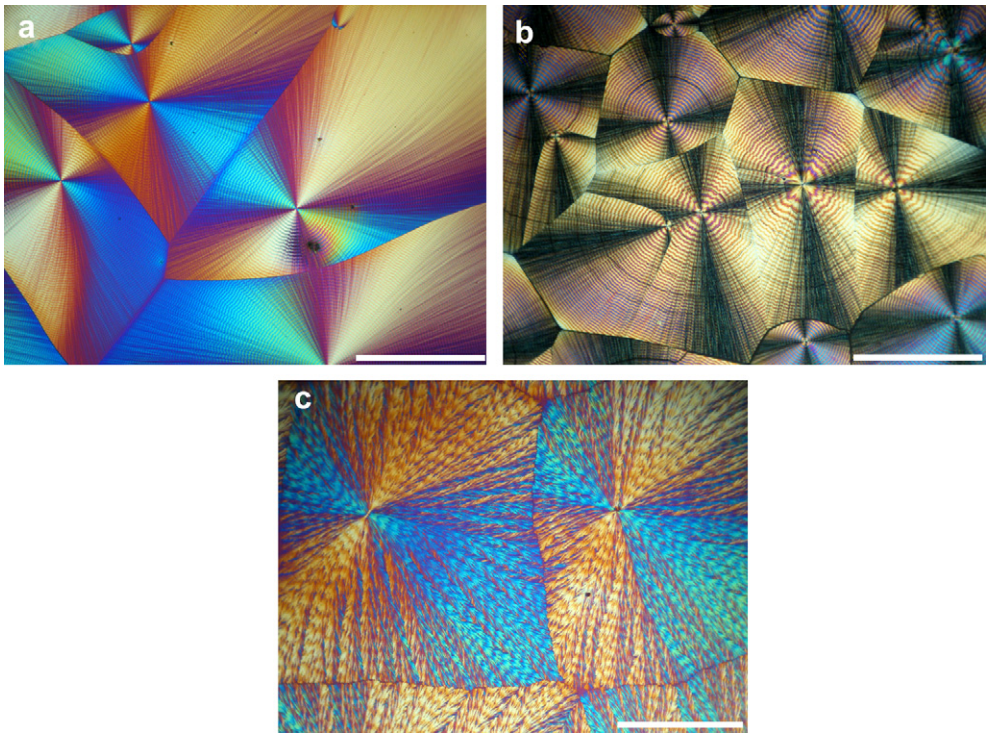

Fig. 5. POM micrographs of A0 (a), A1 (b) and A2 (c) isothermally crystallized at 150 °C for 30 min. The scale bar represents 100 μm.

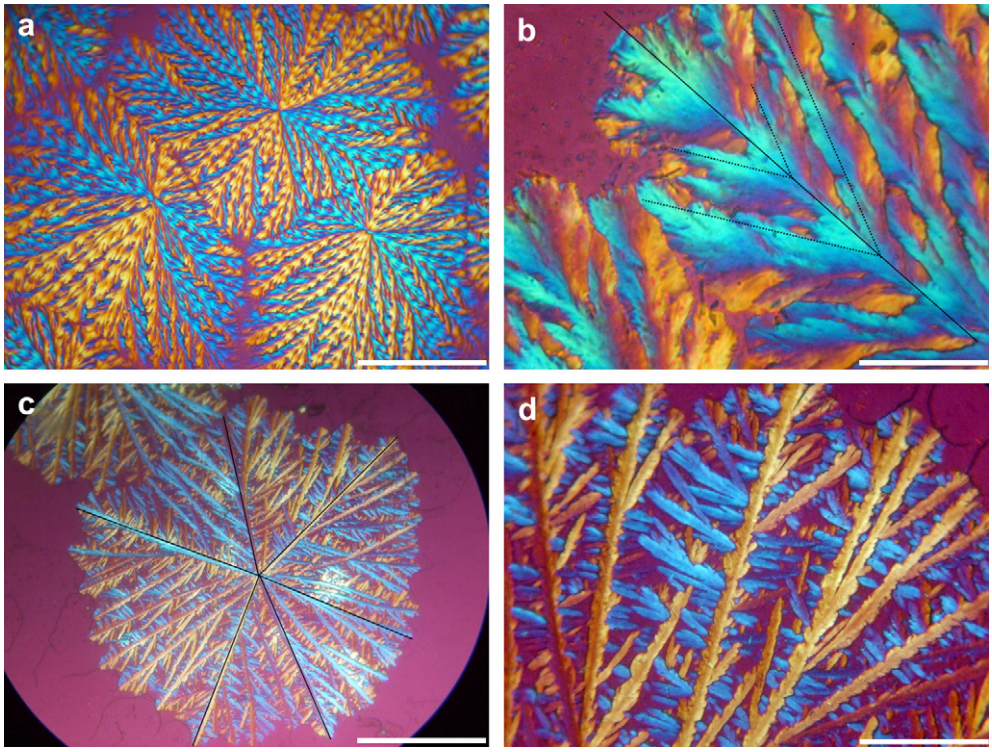

Fig. 6. POM micrographs of A2 crystallized at 150 °C for 30 min. The film thickness of (a) and (c) are 8 and 2 μm. (b) and (d) are magnification of (a) and (c), respectively. The scale bar in (a), (c) and (b), (d) represent 100 and 20 μm, respectively.

observation, it is recognized that there are some difference between the spherulites in Fig. 5(c) and (b), that is, spherulites in Fig. 5(c) show wheatear-like structure while spherulites in Fig. 5(b) show ring-banded. Ring-banded spherulites are usually observed in pure PTT whereas wheatear-like spherulites has never been found.

To further reveal the wheatear-like spherulites structure, the film thickness of A2 is decreased to 8.0 μm and the POM micrograph is shown in Fig. 6(a). Fig. 6(a) presents the spherulites with sparse stems compared with that in Fig. 5(c), presumably because there is less melts available for crystallization in thin film than in thick film. However, overgrowth lamellae are still observed. The sparse spherulites in Fig. 6(a) are somewhat similar to the previous reported seaweed [33–35]. They have some common character, such as irregular branches and the splitting of growing tips. Here, we call this pattern compact seaweed. Fig. 6(b) is a magnification of Fig. 6(a). From Fig. 6(b), we can clearly see the slitting tips, which suggest that crystal growth loses anisotropy. Based on a careful observation, we can find that the crystals consist of main branches (as indicated by the solid line) and side branches crystals (as indicated by the dot line). During crystals growth, main branches continuously slit and form new side branches. The main branches and the side branches are all composed of lamellar crystals. Lamellar orientation usually changes from edge-on to flat-on, or vice versa in thicker film [36]. Once in a while, some edge-on crystal may grow protrudently from the molten polymer surface.

The sample used in Fig. 6(a) was directly sputtered with a gold layer for SEM observation and the SEM micrographs are presented in Fig. 7. Actually, during hard segment crystallization, crystalline lamellae develop in the amorphous matrix. As a result, the amorphous layers cover the upper and lateral surface of crystals (as shown in Fig. 8), so only the protrudent crystals can be observed by SEM. As shown in Fig. 7, a ribbon-like texture with slitting tips protrudes from the surface and its width is 500–1500 nm. It is undoubtable that Atomic Force Microscopy is a widely accepted useful technology to investigate the surface of the material. However, the crystalline are covered by thick amorphous phase and the image is blurred, so AFM image is not presented in this paper.

Form the above discussion, we speculate that the foregoing wheatear-like structure is a more compact seaweed structure. The decreased film thickness restrains the overgrowths of lamellar crystals, which exhibits a relatively clear crystal assembly.

With further decreasing film thickness of A2 down to 2.0 μm, Fig. 6(c) exhibits a spherulite texture much different from that in Fig. 6(a). The radialized branches in Fig. 6(c) can be clearly distinguished, which is much thinner than that in Fig. 6(a). This observation indicates that the overgrowths do not overlap due to

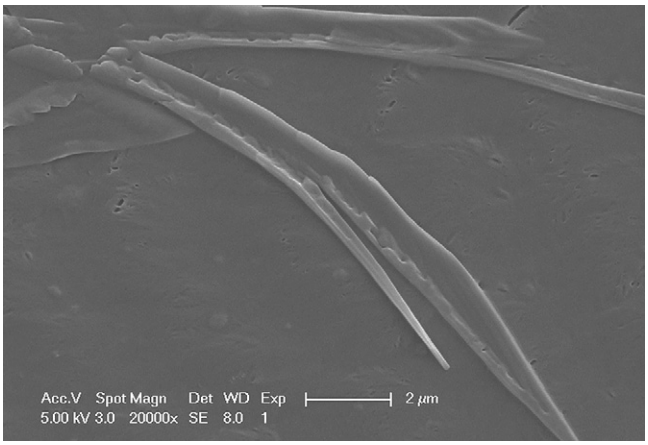

Fig. 7. SEM micrographs of A2 crystallization film surface.

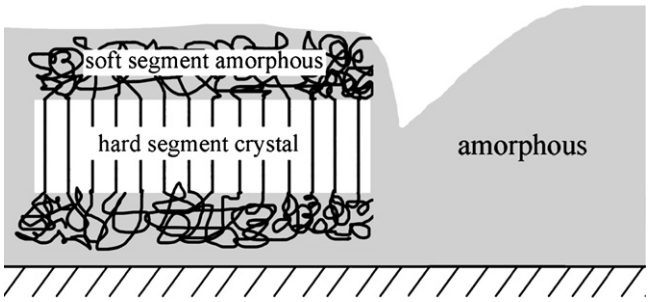

Fig. 8. Schematic illustrations of organization of amorphous and crystal during crystallization.

a decrease of the available polymer melt for crystallization. This type of spherulites has several distinct main branches (as indicated by the solid line) and a large number of side branches. Here, we call it dendritic spherulite. Fig. 6(d) is a magnification of Fig. 6(c). Several main branches and some long or short side branches are clearly observed. It is interesting to find that the short side branches are all perpendicular to the main branches, while the long side branches are nonorthogonal to main branches. We speculate that the side branches grow perpendicularly to the main branches until they encounter impediment, that is, the angles between main and side branches can be changed when the growing side branches encounter impediment. The branches in Fig. 6(d) have a width of 1–2 μm.

Actually, it is not surprising to observe spherulites superstructure in segmented block copolymers. In the case of poly(ether–ester) with PET as rigid segments, Luo et al. [37] and Wang et al. [38] observed the spherulites with distinguishable extinction cross. However, no seaweed and dendritic crystallization morphologies were found. As for PBT, the flexible molecular chain (compared with PBT and PTT) leads to a higher crystallization rate, which makes the size of its spherulite too small to be observed under the resolution of POM. Therefore, no distinct morphology, even spherulite has been reported until recently.

Dendritic growth with apparent crystallographic branching has recently been reported for a number of melt-crystallized polymers in thin or ultrathin films, including poly ethylene (PE) [39], isotactic polystyrene (iPS) [40–42], poly(ethylene oxide) (PEO) [33,43], poly(caprolactone) [44,45], and poly(ethylene oxide) (PEO)/poly(methyl methacrylate) (PMMA) blends [34,35,46,47]. Diffusion of heat or solute away from the growth front is an important aspect of the dendritic growth process. When the effect of thermodynamic driving force for crystallization becomes strong or impurities are added to the system, the crystallization front becomes unstable, and flat interfaces and regular crystal patterns give way to dendritic branching patterns [47].

Up to now, different patterns, such as dendrite, seaweed and compact structure has been successfully represented by computer simulations mainly based on the diffusion-limited aggregation (DLA) mechanism but in consideration of different boundary conditions, such as anisotropy strength, supercooling, surface tension, diffusivity, etc. [48,49]. The underlying DLA model can correctly describe the fractality of the crystal patterns, regarding as the most principal feature. This model is based on the assumption that sticking probability of the particles arriving at the surface of crystals is quite high (close to one), meaning that the particles (or molecules in this study) have no chance to select the correct sites to join the growing crystal front when they have arrived at the interfacial area between solid and liquid. The formation of different patterns attributes to the changes of boundary conditions, which can affect the stacking probability more or less [33,50,51].

In PTT/PEOT segmented copolymers, the amorphous soft phase can be seen as an inherent impurity for crystallized hard phase, and it offers an instinctive effect on the surface tension and diffusivity. In other words, with increasing soft segment content, the surface tension decreases (surface tension related to the density of material. The hard segment and soft segment have different density. It is 1.40 and 1.21 g/cm^3, respectively) and diffusivity increases (because

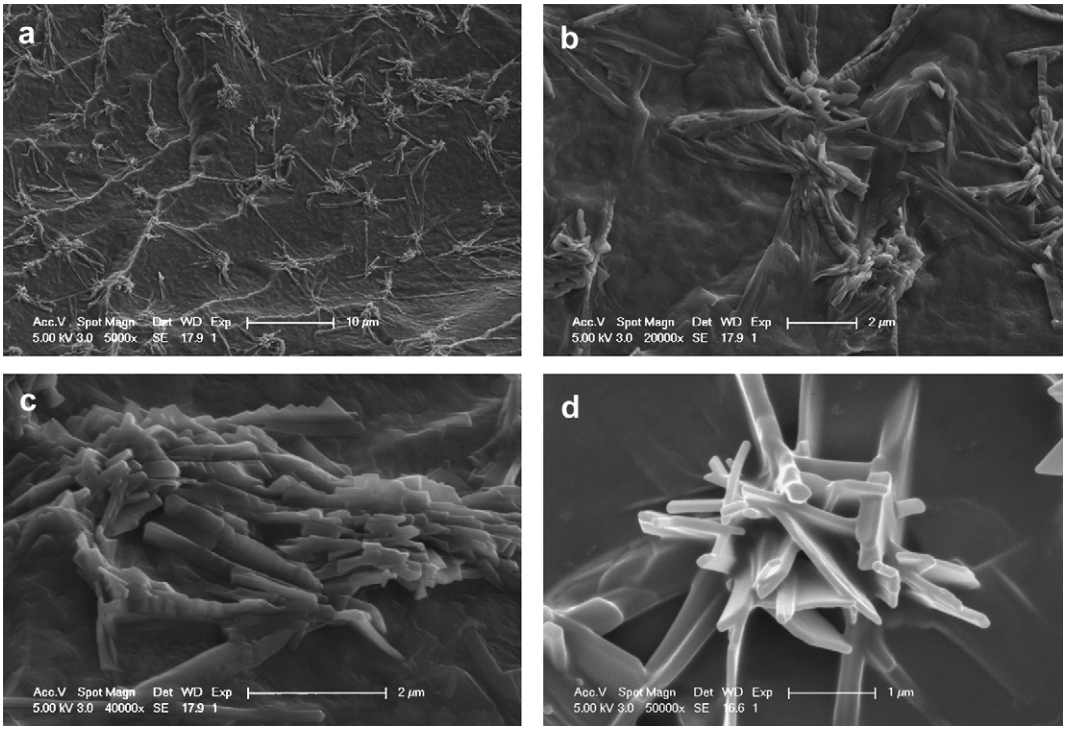

Fig. 9. (a) Micrograph of A2 after crystallizing at 150 °C for 5 h. (d) Brittle fractured surfaces of A2 after stretching. (b) and (c) are magnification of (a).

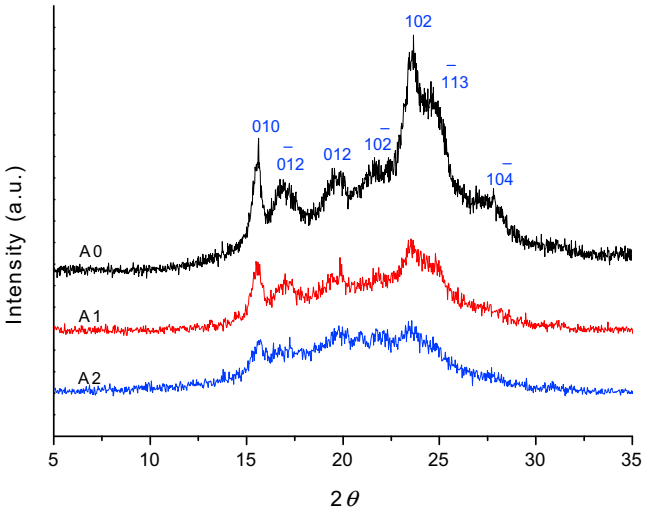

Fig. 10. WAXD patterns for PTT and PTT/PEOT copolymers.

soft segment has lower viscosity than hard segment at the same temperature), which leads to the transformation from regular spherulites to dendritic (or compact seaweed) morphology. The dendritic growth process can be described as follows. During crystallization, the amorphous phase is rejected from the growth front of PTT. Because of the low T_m (19.3 °C) of soft segment and high crystallization temperature (150 °C), crystallization in this system can be viewed as a solution growth process where the buildup of impurities at the growth front drives the breakdown of faceted crystals into dendritic morphologies. Several previous papers about PEO/PMMA blends could be taken as reference [37,47]. In their work, crystallized PEO was deliberately mixed with amorphous PMMA to "tune" its morphology. With increasing PMMA content, the spherulitic morphology transformed into a symmetric dendritic morphology. It is reasonable to claim the effect of PEOT soft segment in PTT/PEOT segmented copolymers is similar to that of amorphous PMMA in PEO/PMMA blends.

The same block copolymer can exhibit different morphologies depending on sample thickness [52]. In the case of A2, with decreasing film thickness from 15 to 2 μm, the morphology changes from wheatear-like, compact seaweed to dendritic. We considered that there are more melts available for crystallization in thick films so overgrowth lamellae are promoted, and vice versa.

3.4. Crystal in the bulk

The hard segments of PTT/PEOT segmented copolymers can be crystallized not only in thin film but also in the bulk. Fig. 9 shows the SEM micrographs of A2 which crystallized at 150 °C for 5 h and stretched. It is interesting to find that many flower-like crystals dispersed uniformly on the brittle fractured surface, and they are surrounded by amorphous material (Fig. 9(a)). The fine structure of the crystals is best resolved in Fig. 9(b). It appears that the petal-like crystals consist of several radialized petal-like arms and a more densely packed center. The arms have a width of 350–500 nm which is a little smaller than that found in thin film (i.e., Fig. 7). The center of crystal can be better resolved in high-resolution as shown in Fig. 9(c). It can be found that the center is composed of many close-packed lamellar slices which have a thickness of about 40 nm. The arms and center of the crystals are supposed to consist of almost pure hard segments. However, due to interconnectivity of the hard and soft segments, they may contain some soft segments [3].

It is well-known that crystallization has a tremendous influence on properties and applications of materials. Considering the situation in TPEs, hard segments play the role of physical cross-links, acting as high modulus filler and offering strength for the polymer. As seen in Fig. 9(a) and (b), the crystallization of hard segments is very similar to fillers and they have strong interfacial interaction to the matrix. When the material is subjected to tense, the crystals will act as stress concentrators. Consequently, deformation and debonding will be found at the interface, as seen in Fig. 9 (d). However, the crystallization in PTT/PEOT has a lager size than in other TPE [3], which would exert a negative effect on the toughness of TPEs. More details on the relationship between crystallization morphology and performance (i.e., mechanical properties) of PTT/PEOT are in progress and will be reported in the subsequent publication.

3.5. Wide-angle X-ray diffraction analysis

The crystal structure of PTT and the block copolymers crystallized at 150 °C for 5 h are observed by using WAXD and the results are shown in Fig. 10. The intensity of scattering is plotted as function of 2θ and the crystal lattice is also designated [26]. Fig. 10 shows that these samples exhibit similar diffraction patterns, implying that the crystal lattices of these samples do not change. In other words, only one crystal structure exists in these copolymers. The reason is that, the crystallization temperature is 150 °C, which is higher the T_m of soft segment, so only the hard segment can crystallize. The results indicate that the above mentioned ring-banded spherulites, wheatear-like, compact seaweed and dendritic morphology have the same crystal lattices as PTT. In fact, PTT could also show both regular and banded spherulites under different boundary condition (i.e., supercooling) while keeping the same crystal structure [27,53]. Moreover, the intensity of diffraction peak gradually decreased with increasing soft segment content, which results from the decreases in the length of the rigid segments.

4. Conclusions

Two kinds of segmented poly(ether–ester) based on poly(trimethylene terephthalate) as rigid segments and poly (ethylene oxide terephthalate) as soft segments were synthesized. ^{1}H NMR spectra was employed to determine the resultant hard segment content. DSC measurements revealed that the copolymers containing 35 wt% soft segments showed only an obvious melting temperature, whereas the copolymers containing 57.3 wt% soft segments presented a low glass transition temperature (−46.4 °C) and a high melting temperature (201.8 °C). With increasing soft segment content from 35 to 57 wt%, the crystallization morphology transformed from regular spherulites to compact seaweed morphology at a certain film thickness, which was due to the surface tension and diffusivity was changed with increasing the content of soft segment. Moreover, with decreasing film thickness from 15 to 2 μm, the crystallization morphology of the copolymer (57 wt% soft segment) changes from wheatear-like, compact seaweed to dendritic. SEM micrographs revealed that some flower-like crystals presented in the bulk. The flower-like crystals consist of several radialized petal-like arms and a more densely packed center, which had never been found in the poly(ether–ester) segmented copolymers with PBT and PET serving as rigid segments. WAXD results showed that the ring-banded spherulites, wheatear-like, compact seaweed and dendritic morphology have the same crystal lattices as PTT.

References

[1] Schuur M, Gaymans R. Polymer 2007;48:1998–2006.
[2] Yang I, Tsai PH. J Polym Sci Part B: Polym Phys 2005;43:2557–67.
[3] Petrović ZS, Cho YJ, Javni I, Magonov S, Yerina N, Schaefer DW, et al. Polymer 2004;45:4285–95.
[4] Lohmar J, Meyer K, Goldbach G. Makromol Chem 1988;189:2053–65.
[5] Aneja A, Wilkes GL. Polymer 2003;44:7221–8.
[6] Arun A, Gaymans RJ. Polymer 2008;49:2461–70.
[7] Schuur M, Boer J, Gaymans RJ. Polymer 2005;46:9243–56.
[8] Arun A, Gaymans RJ. Macromol Chem Phys 2008;209:854–63.
[9] Sauer BB, Gaymans RJ, Niesten MCE. J Polym Sci Part B: Polym Phys 2004;42:1783–92.
[10] Krijgsman J, Husken D, Gaymans RJ. Polymer 2003;44:7573–88.
[11] Sun L, Liu Y, Zhu L, Hsiao BS, Avila-Orta CA. Polymer 2004;45:8181–93.
[12] Nojima S, Kiji T, Ohguma Y. Macromolecules 2007;40:7566–72.
[13] Hamley IW, Castelletto V, Castillo RV, Mueller AJ, Martin CM, Pollet E, et al. Macromolecules 2005;38:463–72.
[14] Li LB, Séréro Y, Koch MHJ, de Jeu WH. Macromolecules 2003;36:529–32.
[15] Nojima S, Kato K, Yamamoto S, Ashida T. Macromolecules 1992;25:2237–42.
[16] Piao LH, Dai ZL, Deng MX, Chen XS, Jing XB. Polymer 2003;44:2025–31.
[17] Loo YL, Register RA, Ryan AJ, Dee GT. Macromolecules 2001;34:8968–77.
[18] Loo YL, Register RA, Ryan AJ. Macromolecules 2002;35:2365–74.
[19] Yu PQ, Xie XM, Wang Z, Li HS, Bates FS. Polymer 2006;47:1460–4.
[20] Piao LH, Deng MX, Chen XS, Jiang LS, Jing XB. Polymer 2003;44:2331–6.
[21] Gabriëlse W, Soliman M, Dijkstra K. Macromolecules 2001;34:1685–93.
[22] Schmalz H, Abetz V, Lange R, Soliman M. Macromolecules 2001;34:795–800.
[23] Fakirov S. Handbook of condensation thermoplastic elastomers. Weinheim: Wiley-VCH; 2005 [chapter 3, p. 77–116].
[24] Adams RK, Hoeschele GK, Witsiepe WK. Thermoplastic polyether–ester elastomers. In: Holden G, Kricheldorf HR, Quirk RP, editors. Thermoplastic elastomers. Munich: Hanser; 2004. p. 183–216 [chapter 8].
[25] Chuang WT, Hong PD, Chuah HH. Polymer 2004;45:2413–25.
[26] Wang B, ChY Li, Hanzlicek J, Cheng SZD, Geil PH, Grebowicz J, et al. Polymer 2001;42:7171–80.
[27] Xue ML, Sheng J, Yu YL, Chuah HH. Euro Polym J 2004;40:811–8.
[28] Chen YF, Woo EM, Wu PL. Mater Lett 2007;61:4911–5.
[29] Arnal ML, Balsamo V, Carrasquero FL, Contreras J, Carrillo M, Schmalz H, et al. Macromolecules 2001;34:7973–82.
[30] Yao CG, Yang GS. J Appl Polym Sci 2009;111:1713–9.
[31] Deschamps AA, Grijpma DW, Feijen J. Polymer 2001;42:9335–45.
[32] Szymczyk A. Euro Polym J 2009;45:2653–64.
[33] Zhai X, Wang W, Zhang G, He B. Macromolecules 2006;39:324–9.
[34] Ferreiro V, Douglas JF, Warren JA, Karim A. Phys Rev E 2002;65:042802.
[35] Ferreiro V, Douglas JF, Warren JA, Karim A. Phys Rev E 2002;65:051606.
[36] Kikkawa Y, Abe H, Fujita M, Iwata T, Inoue Y, Doi Y. Macromol Chem Phys 2003;204:1822–31.
[37] Luo XL, Zhang XY, Wang MT, Ma DZ, Xu M, Li FK. J Appl Polym Sci 1997;64:2433–40.
[38] Wang MT, Zhang LD, Ma DZ. Euro Polym J 1999;35:1335–43.
[39] Zhang F, Liu J, Huang H, Du B, He T. Eur Phys J E 2002;8:289–97.
[40] Taguchi K, Miyaji H, Izumi K, Hoshino A, Miyamoto Y, Kokawa R. Polymer 2001;42:7443–7.
[41] Beers KL, Douglas JF, Amis EJ, Karim A. Langmuir 2003;19:3935–40.
[42] Taguchi K, Toda A, Miyamoto YJ. Macromol Sci Phys 2006;45:1141–7.
[43] Reiter Günter, Strobl Gert R. Progress in understanding of polymer crystallization. Berlin Heidelberg: Springer; 2007 [chapter 18].
[44] Mareau VH, Prud'homme RE. Macromolecules 2005;38:398–408.
[45] Mareau VH, Prud'homme RE. Polymer 2005;46:7255–65.
[46] Okerberg BC, Marand H. J Mater Sci 2007;42:4521–9.
[47] Okerberg BC, Marand H, Douglas JF. Polymer 2008;49:579–87.
[48] Bogoyavlenskiy VA, Chernova NA. Phys Rev E 2000;61:1629–33.
[49] Sommer JU, Reiter G. J Chem Phys 2000;112:4384–93.
[50] Eckmann JP, Meakin P, Procaccia I, Zeitak R. Phys Rev Lett 1990;65:52–5.
[51] Ihle T, Müller-Krumbhaar H. Phys Rev Lett 1993;70:3083–6.
[52] Kim G, Han CC, Libera M, Jackson CL. Macromolecules 2001;34:7336–42.
[53] Srimoaon P, Dangseeyun N, Supaphol P. Euro Polym J 2004;40:599–608.